COMMUNICATION

Making soluble Dy_2 single-molecule magnets red emissive through their functionalization by ruthenium–cyanido luminophores

Received 00th January 20xx,
Accepted 00th January 20xx

DOI: 10.1039/x0xx00000x

Michal Liberka[a,b] and Szymon Chorazy*[,a]

We present an efficient strategy for obtaining red-emissive molecular nanomagnets by exploring a heterometallic approach. We report $\{[Dy^{III}(4\text{-pyridone})_5]_2[Ru^{II}(CN)_2(phen)_2]_2\}\cdot(CF_3SO_3)_6\cdot 2MeOH$ (phen = 1,10-phenanthroline) compound composed of exchange-coupled $\{Dy^{III}_2\}$ single-molecule magnets functionalized by Ru(II)-cyanido units. The latter makes the resulting $\{Dy^{III}_2Ru^{II}_2\}^{6+}$ cations a unique example of a soluble lanthanide SMM exhibiting red charge-transfer photoluminescence in the solution and solid state, well enhanced when compared with the cyanido precursor.

Red-emitting materials have aroused much attention because of their applications in night vision, biomedical imaging, optical communication, computing, and light-emitting diodes (LEDs).[1] In the last few years, large efforts have been devoted to the design of red phosphors, however, it remains a great issue to achieve efficient red emission since the fundamental limitation of the energy-gap theory.[2] Most red light-emitting materials include QDs and transition-metal/rare-earth phosphors, such as K_2TiF_6:Mn^{4+} and $CaAlSiN_3$:Ce^{3+} orange-red phosphors or $CsPbI_3$ quantum dots.[3] The stringent conditions for the synthesis of fluoride and azide materials limit their easy use for everyday applications while high-performance monochromatic QDs have often poor thermal stability and susceptibility to humidity in the environment. This can be overcome by perovskite materials or transition-metal complexes but, in this context, there the related strategies are still needed.[4]

Besides the quest for better performance and processable solid light emitters, research focused on the functionalization of materials to achieve multifunctional luminophores attracted broad attention, especially as it was found designable using a molecular building block approach.[5] In this context, proton conductive, chiral, or ferroelectric luminophores were reported.[6] Moreover, emissive single-molecule magnets (SMMs), exhibiting strong magnetic anisotropy, leading to the slow relaxation of magnetization and a magnetic hysteresis loop, appear as a promising possibility.[7] They are considered for applications in LEDs or sensing when their optical side is explored, whereas, within the field of molecular magnets, they are applicable for data storage, quantum computing, or spintronics, offering also useful opto-magnetic correlations.[8]

Although a considerable number of luminescent SMMs were reported,[7] the strategy for red-emitting SMMs is to be developed. One may consider introducing a red-emitting organic ligand to the lanthanide(III) (Ln) SMM but, often, it leads to the antenna effect and enhancement of 4f emission.[7d] On the other hand, inorganic SMM-based materials might serve as a matrix for red-emissive Eu^{2+}/Eu^{3+}-doped systems but this can be realized only by mixing Ln ions in a solid solution.[9] We decided to address this challenge by exploiting cyanido complexes of transition metals which are efficient metallo-ligands for Ln-SMMs.[7f,10] Cyanido complexes used alone can induce only moderate SMM properties, however, they provide a rigid backbone for f-metal ions and enable control over its SMM effect by organic ligands.[11] Cyanido metal complexes can be emissive, often enhancing the emission of Ln(III) centers.[12] Thus, the related d-f assemblies are good candidates for emissive SMMs, offering also broader multifunctionality.[10] We decided to work with rarely explored red-luminescent Ru(II)-polypyridyl complexes bearing additional cyanido ligands.[13] We focused on *cis*-$[Ru^{II}(CN)_2(phen)_2]$ (phen = 1,10'-phenanthroline), an emissive analog of Fe(II) species which was recently combined by us with Dy(III) centers into a unique vapo-/solvatochromic SMM based on tetranuclear $\{Dy^{III}_2Fe^{II}_2\}^{6+}$ ions.[10e] Here, we report $\{[Dy^{III}(4\text{-pyone})_5]_2[Ru^{II}(CN)_2(phen)_2]_2\}\cdot(CF_3SO_3)_6\cdot 2MeOH$ (**Dy_2Ru_2**, 4-pyone = 4-pyridone) molecular system that serves as a soluble exchange-coupled SMM and reveals red emission, enhanced by the coordination of a Ru(II) emitter to the 4f metal ion. These issues were discussed using X-ray diffraction, magnetic, and spectroscopic data.

Crystals of **Dy_2Ru_2** were obtained by the self-assembly of $Dy^{III}(CF_3SO_3)_3$ with *cis*-$[Ru^{II}(CN)_2(phen)_2]$ complexes and excess of 4-pyone in the MeOH/MeCN solution. Their structure could

[a] *Faculty of Chemistry, Jagiellonian University, Gronostajowa 2, 30-387 Krakow, Poland. E-mail: simon.chorazy@uj.edu.pl*
[b] *Doctoral School of Exact and Natural Sciences, Jagiellonian University, Lojasiewicza 11, 30-348 Krakow, Poland*

†Electronic Supplementary Information (ESI) available: Experimental section, EDX and MS analysis, IR spectra, TGA, detailed structural parameters and views, P-XRD patterns, additional magnetic curves, summary of magnetic relaxation parameters, comment on fitting of *ac* magnetic data, UV-vis spectra, additional luminescent characteristics. For ESI see DOI: 10.1039/x0xx00000x

not be determined using the single-crystal X-ray diffraction method, however, it was deduced by isostructurality with the Fe(II)-containing analog **Dy_2Fe_2**,[10e] as suggested by the mass spectroscopy and powder X-ray diffraction method (Fig. 1; Fig. S1 and S5, Table S2), further confirmed by IR spectra, TGA, and elemental analyses (see Experimental section, Fig. S2 and S3). Moreover, we obtained and determined the crystal structure of analogous compounds with the mixed Fe/Ru metal content, i.e., **$Dy_2Fe_{1.2}Ru_{0.8}$** and **$Dy_2Fe_{0.8}Ru_{1.2}$**, which confirmed the isostructurality of these solid solutions with **Dy_2Fe_2** and **Dy_2Ru_2** (Fig. 1; Fig. S1–S5, Tables S1–S6). These experiments reveal that the crystal structure of **Dy_2Ru_2** consists of tetranuclear $\{Dy^{III}_2Ru^{II}_2\}^{6+}$ molecular cations surrounded by triflate anions and some methanol solvent molecules (Fig. 1, and S4). The molecular cation consists of two Dy^{III} centers connected by two bridging 4-pyone ligands. Such a coordination scheme results in a rhombic $\{Dy_2O_2\}$ molecule core with the Dy–Dy distance of ca. 4.1 Å. Perpendicular to organic linkers, Dy^{III} centers coordinate octahedral $[Ru^{II}(CN)_2(phen)_2]$ by cyanido bridges. Due to the angular coordination of CN^- -bridges, the resulting tetranuclear ion is bent with two terminal complexes oriented oppositely. The coordination sphere of Dy^{III} complexes is completed with four additional 4-pyone ligands, leading to a seven-coordinated $[Dy^{III}(NC)(4\text{-pyone})_6]^{3+}$ complex of a nearly perfect pentagonal bipyramidal (D_{5h}) geometry (Fig. 1, and Table S5). Its equatorial base is formed by two bridging and two non-bridging O-atoms of 4-pyone ligands as well as a cyanido N-atom. The two remaining O-atoms are located in the axial positions and are characterized by a much shorter bond distance to the metal ion, ca. 2.22–2.25 Å when compared to atoms in equatorial positions, while the vertical O–Dy–O angle slightly exceeds 172°. The aromatic rings of organic ligands participate in inter- and intra-molecular π–π interactions, stabilizing the supramolecular framework together with H-bonds between 4-pyone and triflate units. It is important to underline here that ESI-MS spectra prove the existence of $\{Dy^{III}_2Ru^{II}_2\}^{6+}$ molecular cations in the MeOH solution of **Dy_2Ru_2** as well as the mixture of $\{Dy^{III}_2Ru^{II}_2\}^{6+}$, $\{Dy^{III}_2Fe^{II}_2\}^{6+}$, and $\{Dy^{III}_2Fe^{II}_1Ru^{II}_1\}^{6+}$ in the trimetallic analogs.

The direct-current (*dc*) magnetism for **Dy_2Ru_2** is gathered in Fig. S6. The decreasing course of χT product upon cooling is related to the thermal depopulation of higher-lying m_J sublevels of the $^6H_{15/2}$ ground Dy^{III} multiplet while, at the very low-*T*, the magnetic exchange within 4-pyone-bridged Dy^{III}_2 pair starts to operate. The related interaction is, however, weak as was discussed previously for **Dy_2Fe_2**, whereas the other magnetic interactions in the structure can be surely neglected due to the diamagnetic Ru(II) complexes isolating the mentioned Dy^{III}_2 units.[10e] The alternate-current (*ac*) magnetism is presented in Fig. 2 and S7–S8, Table S7. Under zero-*dc*-field, **Dy_2Ru_2** exhibits pronounced slow relaxation of magnetization represented by maxima on the $\chi''(\nu)$ plots (Fig. 2a). Up to 2 K, they appear even below 1 Hz and shift to higher frequencies with heating. In the range of 0.1–1000 Hz, the detectable *ac* signal was found from 2 K to 14 K and was analyzed by a generalized Debye model for a single relaxation process in the 2.5–10 K range. Upon the application of non-

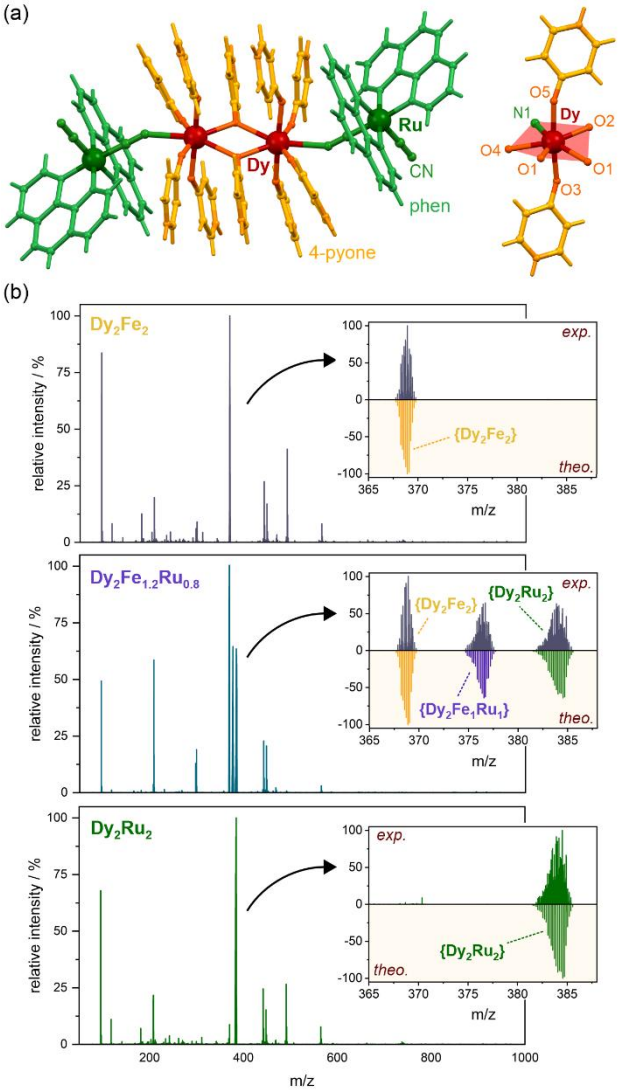

Fig. 1 The structure of $\{Dy^{III}_2Ru^{II}_2\}^{6+}$ molecular cations of **Dy_2Ru_2** visualized using the crystal structure of isostructural **$Dy_2Fe_{1.2}Ru_{0.8}$**, shown with the insight into the Dy(III) complex with the indicated equatorial plane of a pentagonal bipyramidal geometry (a), and the ESI-MS spectrum of **Dy_2Ru_2** compared with those of **Dy_2Fe_2** and **$Dy_2Fe_{1.2}Ru_{0.8}$** (positive ion mode) with the enlargement of the region related to the the presence of $\{[Dy(4\text{-pyone})_5]_2[Fe(CN)_2(phen)_2]_2\}^{6+}$ (orange), $\{[Dy(4\text{-pyone})_5]_2[Fe(CN)_2(phen)_2]_1[Ru(CN)_2(phen)_2]_1\}^{6+}$ (violet), and $\{[Dy(4\text{-pyone})_5]_2[Ru(CN)_2(phen)_2]_2\}^{6+}$ (green) fragments.

zero *dc* fields, the maxima in the $\chi''(\nu)$ plots remain almost in the same range until ca. 600 Oe, after which they are shifted to higher frequencies due to a field-induced direct relaxation (Fig. S7). This behavior indicated the small contribution of quantum tunneling of magnetization (QTM) within the almost pure ground Kramers doublet, which was also found for **Dy_2Fe_2** analog.[10e] Under the *dc* field of 600 Oe, the maxima are only slightly shifted toward the lowest frequencies and could be also analyzed by a generalized Debye model in the 3.5–10 K range. Extracted relaxation times were analyzed using the simultaneous 3-D fitting based on all obtained curves, $\tau(T, H)$, using *relACs* program, taking into account direct, Raman, Orbach, and QTM processes (see Fig. S7–S8, Table S7, and the related comment in ESI).[11] Firstly, the energy barrier values of the Orbach process (285 K) were taken from the *ab initio*

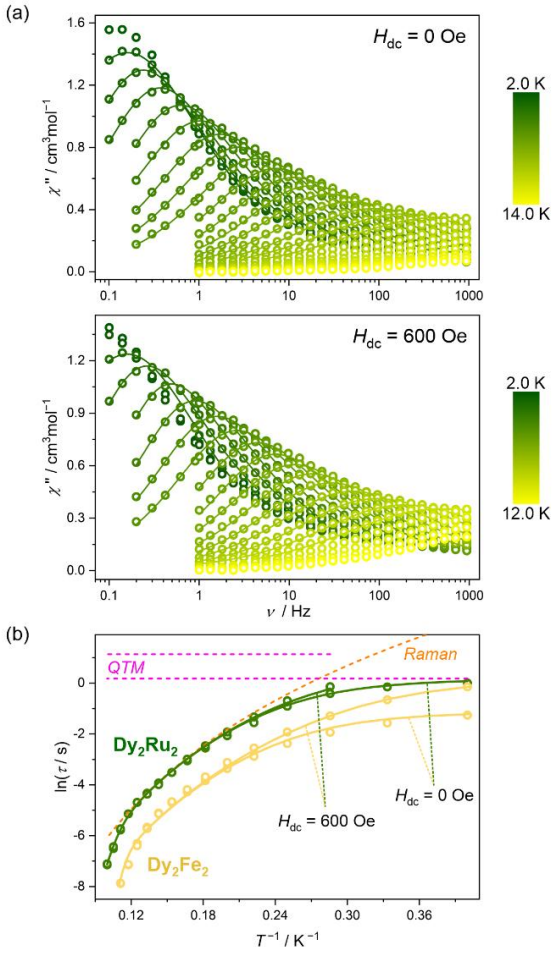

Fig. 2 Alternate-current (*ac*) magnetism of **Dy_2Ru_2**: the frequency dependences of out-of-phase susceptibility, χ'', for the indicated temperature range at H_{dc} of 0 Oe and 600 Oe, shown together with the fitting to the Debye model (solid lines) (a), and the *T*-dependences of resulting relaxation times, compared with the *T*-dependences of relaxation time determined for the **Dy_2Fe_2** analog (b).[10e] In (b), the circle points show the experimental data, solid red lines show the best-fit curves obtained taking into account the combined contributions from direct, Raman, QTM, and Orbach processes, while dashed colored lines show the separate contributions from selected processes.

calculations performed for **Dy_2Fe_2**, which allowed us to obtain reasonable physical parameters of the relaxation processes (Fig. 2b, Table S7).[10e] An alternative fit without fixing the Orbach energy barrier was also performed, and the extracted value of the thermal energy barrier is 313 K, which suggests only a small influence of the diamagnetic metal ion on the single-ion anisotropy of Dy(III). This is also supported by rather subtle changes in the Dy(III) coordination sphere in **$Dy_2Fe_xRu_{2-x}$** (Tables S4–S5). In the widest *T*-range, the magnetic relaxation is dominated by the Raman process (Fig. 2b), thus the varying parameters related to this path represent the modulation of the slow magnetic relaxation by the diamagnetic ion change (Table S7). Both **Dy_2Re_2** and **Dy_2Fe_2** are characterized by a similar value of the Raman relaxation B_{Raman} parameter, which may be associated with a similar number of available phonon modes in these systems.[8,10,11] This is not surprising as they are isostructural having the analogous set of molecular units. However, the replacement of lighter $[Fe^{II}(CN)_2(phen)_2]$ with heavier $[Ru^{II}(CN)_2(phen)_2]$ complexes has a significant impact on the energy of critical vibrational modes, as reflected by the power *n*, much higher in **Dy_2Ru_2** than in **Dy_2Fe_2**.[10e]

Concerning the photophysics, first of all, UV-vis absorption spectra of **Dy_2Ru_2** in MeOH consists of one broad band in the range of 330–550 that coincides with the spectrum of the $[Ru^{II}(CN)_2(phen)_2]$ (Fig. S9). This absorption is broader in the solid and associated with the Ru-to-phen charge transfer (MLCT) transition.[13] Absorption in the higher energy range below 300 nm is related to the contributions from the MLCT and ligand-field electronic transitions within Ru^{II} complexes, as well as spin-allowed transitions of organic ligands. Both **Dy_2Ru_2** and $[Ru^{II}(CN)_2(phen)_2]$ show a deep red broadband emission (550–850 nm) in the MeOH solution under the UV excitation, with maximum centered at ca. 673 nm (Fig. 3, S10–S11 and Table S8). This luminescence is characterized by a similar lifetime of ca. 80 ns and a similar excitation spectrum overlapping with the absorption. These properties are expected for Ru(II)-polypyridyl complexes and can be attributed to the emission from the lowest excited triplet MLCT state.[13] In a solid state, the room-temperature emission spectrum of **Dy_2Ru_2** is in the same position as in solution but is narrower with a maximum at 683 nm (Fig. 3). More importantly, there is a significant blueshift going from the precursor to **Dy_2Ru_2**. The excitation spectrum consists of a set of bands in the 300–640 nm range. Compared to the $[Ru^{II}(CN)_2(phen)_2]$, both emission and excitation spectra are shifted to higher energies. At low temperatures, the emission band range narrows and falls in the 600–800 nm range with the maximum at 675 nm and slightly outlined vibrational progression. Compared to the Ru^{II} precursor, there is a slightly smaller shift of bands with a temperature change. The shift of the excitation and emission bands in **Dy_2Ru_2**, when compared with the precursor, is related to the coordination of the cyanido ligand to the Dy^{III} center. This interaction shifts electron density on the CN^- ligand and increases the metal-to-ligand π back-donation.[13] The highest occupied molecular orbitals of mixed Ru *d* (t_{2g}) and cyanido π^* character are therefore stabilized relative to the lowest unoccupied molecular orbitals of phen ligand π^* character, resulting in a net destabilization of MLCT excited states. This increases the energy gap between the ground state located on Ru^{II} and the MLCT excited states, which causes a blueshift of absorption and emission. The efficient luminescence of **Dy_2Ru_2** is demonstrated by the room temperature absolute quantum yield of ca. 23%, incomparably exceeding the yields obtained for $[Ru^{II}(CN)_2(phen)_2]$ and most of the reported Ru(II)-based complexes.[13] Moreover, the emission lifetime of **Dy_2Ru_2** is more than twice as long (252 ns) at room temperature as those of the precursor (107 ns), even though the hetero-metallic **Dy_2Ru_2** contains more high-energy O–H and N–H oscillators. At low temperatures, this difference is smaller, but **Dy_2Ru_2** still has a longer lifetime (almost 1 µs), which proves the enhancement of luminescent properties by coordination.

In summary, we report a convenient strategy for soluble red-emissive Dy(III) SMMs. This was achieved by the pioneering application of cyanido-Ru(II)-polypyridyl complexes as metalloligands for the functionalization of Ln(III) molecular nanomagnets.[7f] The unusual stability of the resulting species in

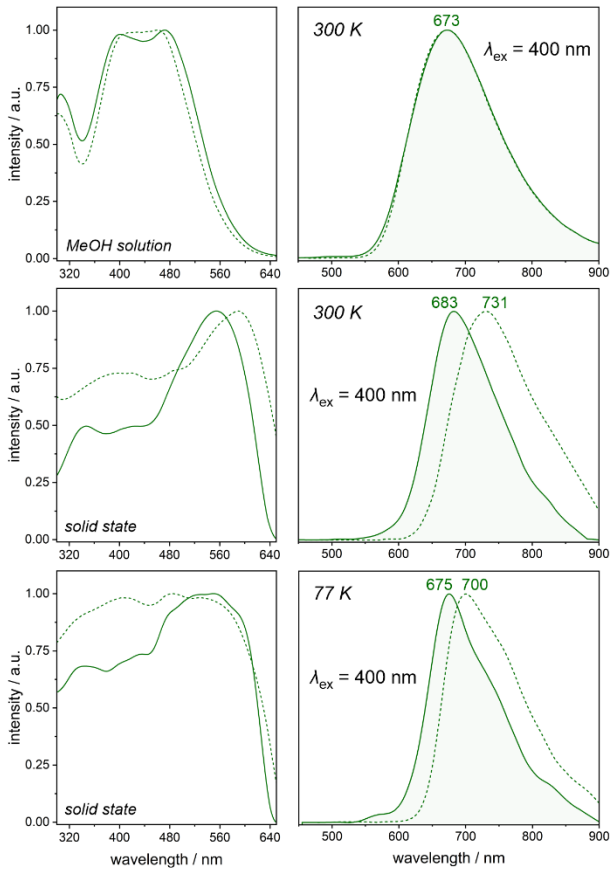

Fig. 3 Comparison of the photoluminescent properties of Dy_2Ru_2 (solid green lines) and $[Ru^{II}(CN)_2(phen)_2]$ precursor (dashed green lines), including the excitation and emission spectra in the MeOH solution and the solid-state at the indicated temperatures. The excitation spectra were collected for the indicated emission maxima.

the solution, observed even for our case in which we used a neutral Ru(II) complex, indicates that the Ln–NC–Ru linkage is surprisingly strong. It opens a broad perspective on the functionalization of various Ln-SMMs by this optically non-innocent Ru(II) metalloligand. Moreover, the employed Ru(II) complexes can be modified through the polypyridyl part which can modulate their optical properties, potentially introducing also other features, such as chirality or enhanced responsivity to chemical stimuli. This pathway towards new multifunctional Ln-SMMs is currently being examined in our laboratory.

This work was financed by the National Science Centre, Poland within the OPUS-21 project, grant no. 2021/41/B/ST5/02544.

References

1 (*a*) Z. Pan, Y.-Y. Lu and F. Liu, *Nat.Mater.*, 2012, **11**, 58; (*b*) A. Abdukayum, J.-T. Chen, Q. Zhao and X.-P. Yan, *J. Am. Chem. Soc.*, 2013, **135**, 14125; (*c*) A. Shao, Y. Xie, S. Zhu, J. Guo, P. Shi, T. D. James, H. Tian and W. H. Zhu, *Angew. Chem., Int. Ed*., 2015, **54**, 7275.

2 (*a*) T. Yang, Z. Cheng, Z. Li, J. Liang, Y. Xu, C. Li and Y. Wang, *Adv. Funct. Mater.*, 2020, **30**, 2002681; (*b*) Y. Zhang, D. Zhang, T. Huang, A. J. Gillett, Y. Liu, D. Hu, L. Cui, Z. Bin, G. Li, J. Wei and L. Duan, *Angew. Chem. Int. Ed*., 2021, **60**, 20498.

3 (*a*) H. Zhu, C. C. Lin, W Luo, S. Shu, Z Liu, Y. Liu, J. Kong, E. Ma, Y. Cao, R.-S. Liu and X. Chen, *Nat. Commun*., 2014, **5**, 4312; (*b*) Y. Q. Li, N. Hirosaki R. J. Xie, T. Takeda and M. Mitomo, *Chem. Mater*., 2008, **20**, 6704.

4 (*a*) S. Chatterjee and A. J. Pal, *J. Mater. Chem. A*, 2018, **6**, 3793; (*b*) E. Kabir, Y. Wu, S. Sittel, B.-L. Nguyen and T. S. Teets, *Inorg. Chem. Front*., 2020, **7**, 1362; (*c*) P. Mandapati, J. D. Braun, I. B. Lozada, J. A. G. Williams and D. E. Herbert, *Inorg. Chem.*, 2020, **59**, 12509; (*d*) L. Schmid, C. Kerzig, A. Prescimone and O. S. Wenger, *JACS Au*, 2021, **1**, 819.

5 (*a*) W. Luo, Y. Tang, X. Zhang, Z. Wu and G. Wang, *Adv. Opt. Mater*., 2023, **11**, 2202259; (*b*) B. Xiong, L. Deng, R. Peng and Y. Liu, *Nanoscale Adv.*, 2019, **1**, 3786.

6 (*a*) J. Long, J. Rouquette, J.-M. Thibaud, R. A. S. Ferreira, L. D. Carlos, B. Donnadieu, V. Vieru, L. F. Chibotaru, L. Konczewicz, J. Haines, Y. Guari and J. Larionova, *Angew. Chem., Int. Ed*., 2015, **54**, 2236; (*b*) J. Wang, J. J. Zakrzewski, M. Heczko, M. Zychowicz, K. Nakagawa, K. Nakabayashi, B. Sieklucka, S. Chorazy and S. Ohkoshi, *J. Am. Chem. Soc*., 2020, **142**, 3970; (c) K. Dhbaibi, M. Grasser, H. Douib, V. Dorcet, O. Cador, N. Vanthuyne, F. Riober, O. Maury, S. Guy, A. Bensalah-Ledoux, B. Baguenard, G. L. J. A. Rikken, C. Train, B. Le Guennic, M. Atzori, F. Pointillart and J. Crassous, *Angew. Chem. Int. Ed*., 2023, **62**, e20221558.

7 (*a*) N. Ishikawa, M. Sugita, S. Koshihara and Y. Kaizu, *J. Am. Chem. Soc.*, 2003, **125**, 8694; (*b*) S. K. Gupta and R. Murugavel, *Chem. Commun.,* 2018, **54**, 3685; (*c*) F.-S. Guo, B. M. Day, Y.-C. Chen, M.-L. Tong, A. Mansikkamäki and R. A. Layfield, *Science*, 2018, **362**, 1400; (*d*) R. Marin, G. Brunet and M. Murugesu, *Angew. Chem. Int. Ed.*, 2021, **60**, 1728; (*e*) J. H. Jia, Q.-Q. Li, Y.-C. Chen, J. L. Liu and M.-L. Tong, *Coord. Chem. Rev.*, 2019, **378**, 365; (*f*) R. Jankowski, M. Wyczesany and S. Chorazy, *Chem. Commun.*, 2023, **59**, 5961.

8 (*a*) A. Zabala-Leuona, J. M. Seco and E. Colacio, *Coord. Chem. Rev.*, 2021, **441**, 213984; (*b*) G. Gabarro-Riera, G. Aromi and E. C. Sanudo, *Coord. Chem. Rev.* 2023, **475**, 214858; (*c*) A. Candini, S. Klyatskaya, M. Ruben, W. Wernsdorfer and M. Affronte, *Nano Lett*., 2011, **11**, 2634; (*d*) A. Gaita-Arino, F. Luis, S. Hill and E. Coronado, *Nat. Chem*., 2019, **11**, 301; (*e*) Y.-C. Chen, J.-L. Liu, Y. Lan, Z.-Q. Zhong, A. Mansikkamaki, L. Ungur, Q.-W. Li, J.-H. Jia, L. F. Chibotaru, J.-B. Han, W. Wernsdorfer, X.-M. Chen and M.-L. Tong, *Chem. Eur. J*., 2017, **23**, 5708.

9 (*a*) J. Qiao and Z. Xia, *J. Appl. Phys.*, 2021, **129**, 200903; (*b*) W. Ye, C. Zhao, X Shen, C. Ma, Z. Deng, Y. Li, Y. Wang, C. Zuo, Z Wen, Y. Li, X. Yuan, C. Wang and Y. Cao, *ACS Appl. Electron. Mater.*, 2021, **3**, 1403.

10 (*a*) S. Chorazy, J. Wang and S. Ohkoshi, *Chem. Commun*., 2016, **52**, 10795; (*b*) M. Andruh, *Chem. Comm*un., 2018, **54**, 3559; (*c*) R. Jankowski, J. J. Zakrzewski, M. Zychowicz, J. Wang, Y. Oki, S. Ohkoshi, S. Chorazy and B. Sieklucka, *J. Mater. Chem. C*, 2021, **9**, 10705. (*d*) J. Wang, J. J. Zakrzewski, M. Zychowicz, Y. Xin, H. Tokoro, S. Chorazy and S. Ohkoshi, *Angew. Chem. Int. Ed*., 2023, **62**, e202306372; (*e*) M. Liberka, M. Zychowicz and S. Chorazy, *Inorg. Chem. Front*., 2024, **11**, 2081.

11 M. Liberka, M. Zychowicz, W. Zychowicz and S. Chorazy, *Chem. Commun.*, 2022, **58**, 6381.

12 (*a*) J.-M. Herrera, S. J. A. Pope, H. Adams, S. Faulkner and M. D. Ward, *Inorg. Chem*., 2006, **45**, 3895; (*b*) J. J. Zakrzewski, B. Sieklucka and S. Chorazy, *Inorg. Chem*., 2020, **59**, 1393.

13 (*a*) N. Karaoun and A. K. Renfrew, *Chem. Commun.,* 2015, **51**, 14038; (*b*) I. M. Dixon, E. Lebon, P. Sutra and A. Igau, *Chem. Soc. Rev*., 2009, **38**, 1621; (*c*) J. Shum, P. Kam-Keung Leung and K. Kam-Wing. Lo, *Inorg. Chem.,* 2019, **58**, 2231; (*d*) E. Wachter, D. K. Heidary, B. S. Howerton, S. Parkin and E. C. Glazer, *Chem. Commun*., 2012, **48**, 9649; (*e*) D. Mara, Z. Cai, S. Bonabello, S. Penna, R. Van Deun, P. Deplano, L. Marchio, L. Pilla and F. Artizzu, *Cryst. Growth Des*., 2024, **24**, 3798.